

# Finite Element Analysis in Functional Morphology

BRIAN G. RICHMOND,<sup>1\*</sup> BARTH W. WRIGHT,<sup>1</sup> IAN GROSSE,<sup>2</sup>  
PAUL C. DECHOW,<sup>3</sup> CALLUM F. ROSS,<sup>4</sup> MARK A. SPENCER,<sup>5</sup>  
AND DAVID S. STRAIT<sup>6</sup>

<sup>1</sup>Center for the Advanced Study of Hominid Paleobiology, Department of Anthropology, George Washington University, Washington, District of Columbia

<sup>2</sup>Department of Mechanical and Industrial Engineering, University of Massachusetts, Amherst, Massachusetts

<sup>3</sup>Department of Biomedical Sciences, Baylor College of Dentistry, Texas A&M Health Science Center, Dallas, Texas

<sup>4</sup>Department of Organismal Biology and Anatomy, University of Chicago, Chicago, Illinois

<sup>5</sup>Department of Anthropology, Institute of Human Origins, Arizona State University, Tempe, Arizona

<sup>6</sup>Department of Anthropology, University at Albany, Albany, New York

---

---

## ABSTRACT

This article reviews the fundamental principles of the finite element method and the three basic steps (model creation, solution, and validation and interpretation) involved in using it to examine structural mechanics. Validation is a critical step in the analysis, without which researchers cannot evaluate the extent to which the model represents or is relevant to the real biological condition. We discuss the method's considerable potential as a tool to test biomechanical hypotheses, and major hurdles involved in doing so reliably, from the perspective of researchers interested in functional morphology and paleontology. We conclude with a case study to illustrate how researchers deal with many of the factors and assumptions involved in finite element analysis. © 2005 Wiley-Liss, Inc.

**Key words:** finite-element analysis; mastication; primates; biomechanics; functional morphology; paleoanthropology

---

---

Functional morphologists are often interested in understanding how anatomical structures are deformed by external loads or how well they resist them. Deformation of bone, for example, is an important component of models of bone adaptation (Turner, 1998; Pavalko et al., 2003; Silva et al., 2005, this issue), and comparisons of the ability of bones to resist specific loading regimes are fundamental to studies of form-function relationships in evolutionary biomechanics (Rubin and Lanyon, 1984; Currey, 2002).

Traditional biomechanical methods include theoretical approaches that generate hypotheses (e.g., free body diagrams) and techniques (e.g., force plates, electromyography, pressure pads) that provide information about forces and moments applied to a structure (Preuschoft, 1970; Biewener, 1992; Ruff, 1995). However, this approach provides at best only an approximation of how structures respond under the applied loads, and there are limits to where strain gauges can be placed and they measure strain only in the plane of

the gauge (Hylander, 1984; Dechow and Hylander, 2000; Ross, 2001).

In mechanical terms, the application of a load results in stresses and strains in the structure. Stress ( $\sigma$ ) is defined as force per unit area (F/A) and describes the internal forces in an object (Cowin, 1989; Currey, 2002). Strain ( $\epsilon$ ) describes the deformations that result from an imposed load and is defined as the change in length divided by

---

\*Correspondence to: Brian G. Richmond, Center for the Advanced Study of Hominid Paleobiology, Department of Anthropology, George Washington University, Washington, DC 20052. Fax: 202-994-6079. E-mail: brich@gwu.edu

Received 12 January 2005; Accepted 13 January 2005  
DOI 10.1002/ar.a.20169  
Published online 3 March 2005 in Wiley InterScience  
(www.interscience.wiley.com).

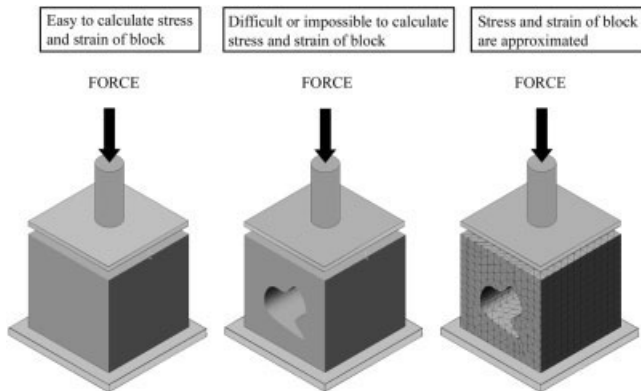


Fig. 1. Problems with simple geometry (left) may easily be solved. More complex shapes (center) are impractical or impossible to solve analytically. The problem may be approximated (right) by subdividing the complex geometry into small elements of simple geometry.

original length ( $\Delta L/L$ ). By convention, stretching a bone in tension is a positive strain and compression is a negative strain.

Stress and strain may be solved exactly by analytical means for simple geometric shapes with homogeneous material properties (Fig. 1). More complex problems are computationally impractical or intractable (Beaupre and Carter, 1992). Even a simple geometry (Fig. 1) cannot be solved analytically if the material properties or loading conditions are complex, as is typically the case with biological structures. The finite element method (FEM) provides an approximate solution to such problems by subdividing the complex geometry into a finite (but typically high) number of elements of simple geometry (Fig. 1).

FEM was first developed as a mathematical technique as early as 1943 (Courant, 1943), but did not see widespread use until the advent of computers. Without computers, FEM was highly impractical and remained ignored until engineers, especially in the aerospace industry, independently developed it later (Levy, 1953). The use of FEM has dramatically increased in the fields of engineering and biomechanics (Huiskes and Chao, 1983). Cook et al. (2001) note that 10 papers using finite elements were published in 1961, 134 in 1966, and 844 in 1971. In 1995, Mackerle (1995) estimated that over 56,000 papers had been published on finite element analysis (FEA), hundreds of books and conference proceedings, as well as the development of 310 general purpose finite element (FE) computer programs. FEM has also become more widely used in the life sciences. A search of the literature in the National Library of Medicine's PubMed database identifies 1 finite-element paper in 1973, 29 in 1983, 91 in 1993, and 457 in 2003.

Although FEA is a powerful tool and growing in popularity, it is important to remember that it is merely a tool. Before considering the best FEM approach, researchers should first decide whether FE modeling is the best method for testing the research questions. Once functional morphologists select FEA, they are faced with numerous decisions about how best to employ it.

Before considering the method's details, we offer definitions of several key terms. The terms "FEM" and "FEA" are often used interchangeably. FEM can be considered

the methodology in which the analysis of interest is converted into a set of algebraic simultaneous equations, whereas FEA refers to the process of analyzing the set of equations. This distinction has little practical impact on those using FEA to examine biological problems, as both processes are embedded in commercial software tools.

The term "FE modeling" refers to the process of creating the model, solving the model, and validating and interpreting the results in the appropriate contexts. In the contexts of functional morphology, creating the model is typically the most time-intensive phase. It involves collecting or integrating data or making assumptions about the model's geometry, mesh and element design, material properties, applied loads, and boundary conditions. The solution phase consists of calculating the stresses and strains that result from the data and assumptions in the model. The last phase, often called the postprocessing phase, involves the interpretation of the results. For biological problems, validation is usually a very important part of this last phase because any interpretations made from the model's results are dependent on the degree to which the model reflects biological reality. Currently, most FEA papers in functional morphology include or cite data that form the bases of modeling decisions (e.g., geometry, material properties, loads, and boundary conditions), but do not provide sufficient evidence to validate their model. Below, we discuss some of the major issues and approaches involved in the three major steps, model creation, solution, and validation and interpretation, of FE modeling (Fig. 2).

## MODEL CREATION

### Geometry

The first step in creating an FE model is deciding on the dimension (1-, 2-, or 3D) of the problem. Higher dimensions, while potentially more realistic, are disproportionately more difficult to model, solve, and subsequently examine, and 2D analyses are often adequate for the questions at hand (Richmond, 1998; Rayfield, 2004). The researcher must also decide on the geometric precision needed to address the questions of interest. Abstract geometric representations are relatively simple to create using computer-automated design (CAD) software. Simple geometric abstractions of real biological structures limit the model's potential and, if too abstract, may not be a valid representation of the real structure's behavior.

To create a realistic geometric model, the geometry of the structure must be input into a computer. A variety of techniques are available, including automated and manual techniques. One automated approach involves transforming laser scans of bones or other structures into wireframe models that are then converted into FE models. Laser scans can offer a high-resolution representation of the outer surface, but lack information about internal geometry (Kappelman, 1998). Computed tomography (CT) scan voxels (3D version of pixels, the unit volume resolution) can also be directly transformed into the elements of a high-resolution FE model (Ryan and van Rietbergen, 2005). The automation and high resolution make this method attractive, but it also involves complex issues in finding appropriate thresholding algorithms to demarcate the bone-air (or other) boundary reliably throughout a structure (e.g., skull) with varying bone thickness and density (Fajardo et al., 2002; Ryan and van Rietbergen, 2005). It also currently results in models with so many

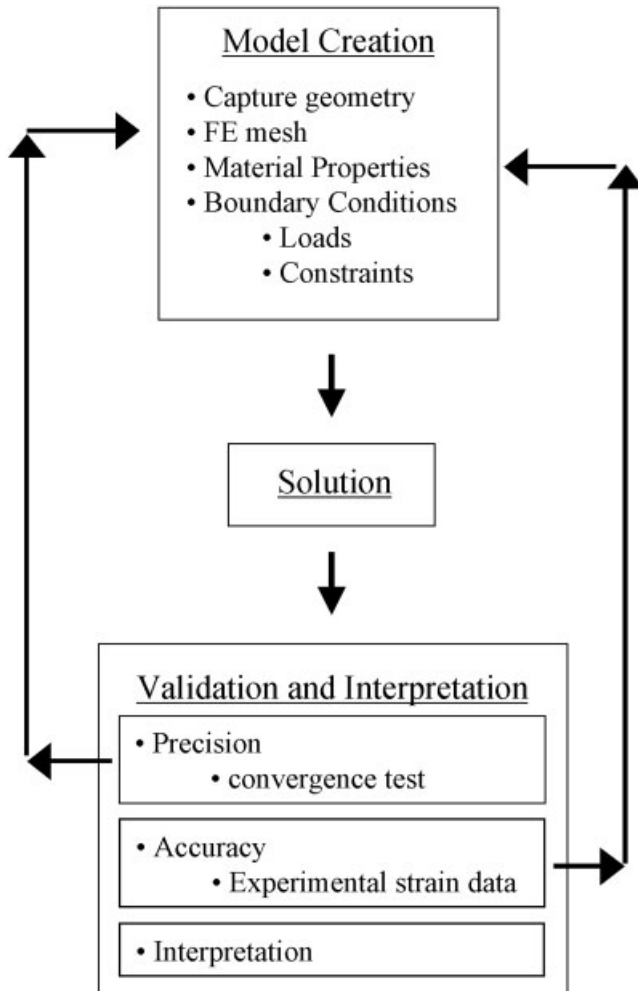


Fig. 2. Schematic diagram of the main steps involved in finite-element modeling.

elements that the models may require computational abilities beyond those available in many powerful desktop workstations.

Images (e.g., photos, CT, MRI) can be manually digitized and made into CAD or other models that FE software can then mesh into FE models. Manual digitization gives the researcher better control over the creation of the model geometry, but involves other thresholding issues (e.g., consistently identifying the bone-air boundary) and can be very time-consuming. We recommend against building 3D models based only on external morphology (e.g., with current laser scanning techniques) in most cases because of the importance of internal structure on the structure's behavior. The researcher's choice of automated versus manual techniques will depend on the researcher's goals and structure of interest.

### Mesh

Transforming the geometry of the physical structure (domain) into an FE model involves subdividing it into a finite, but usually large, number of geometrically simple domains, called finite elements, connected together at

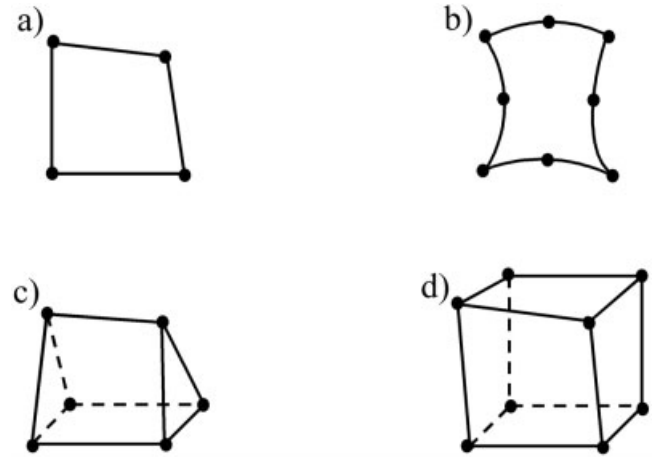


Fig. 3. Several examples of element types. Elements can be linear (a, c, and d) or quadratic (b). The latter are more flexible and accurate, but computationally more expensive. Greater element density also increases accuracy. Typical elements include 2D linear (a) and quadratic (b) elements and 3D polyhedral elements such as the linear six-node wedge (c) and eight-node brick (d) elements.

their vertices, called nodes. The resulting contiguous collection of simply shaped elements connected together by their nodes is called the mesh. A node is a coordinate location in space where degrees of freedom (i.e., displacements) are defined and the displacements are determined in response to the loads (or may be specified a priori). An element refers to the building block of a model and describes how nodes are connected to one another. Each element has mathematical relations that describe how degrees of freedom of one node relate to the next. There are a number of different kinds of elements, depending on the dimensionality of the problem (Fig. 3). A 1D FEA, although rarely performed because of its oversimplification of biological reality, is most conveniently subdivided into a string of connected nodes. Two-dimensional structures are typically meshed with triangular or quadrilateral elements (Fig. 3a and b). These elements may possess two or more nodes per side, with one node at each vertex. If nodes are only placed at the vertices, then the element is called linear because a line function describes the element geometry (Fig. 3), as well as how the displacement field will vary along an element edge. Elements possessing three nodes per side are referred to as quadratic elements. The latter are described by polynomial functions and are therefore generally more precise (the sides may bend and the displacement field may vary quadratically) but also demand more computational time and memory. The exclusive use of linear triangular elements in 2D models is discouraged because, empirically, these models tend to be noticeably less precise than those meshed with other element types (Beaupre and Carter, 1992).

Typical 3D elements include eight-node bricks, six-node wedges, five-node pyramids, and four-node tetrahedra (Fig. 3). With increasing numbers of elements and nodes, the model becomes more complex and computationally more difficult and lengthy. To address this problem, researchers often devise strategies to minimize computational expense, such as taking advantage of symmetry when possible by modeling only half the structure, by

using a generally coarse mesh with finer elements only near regions of geometric complexity or high stress and strain, and/or by using a 2D model when it suffices.

The automated mesh-generating features in most FE software packages produce relatively refined (dense) meshes and can be further refined in regions of interest or throughout the entire model. The mesh generators are also “smart” in that regions likely to undergo high stress concentration and have steep stress gradients are meshed with greater density than other regions, thereby maximizing accuracy and minimizing computational expense.

### Material Properties

Once the mesh is complete, the material properties of the elements must be defined. Depending on the goals of the FEA, a variety of material properties may be modeled, such as heat conductivity, linear and nonlinear elastic properties, and temperature-dependent elastic properties. Functional morphologists are typically interested in the elastic properties of tissues such as bone or enamel that describe how the tissue deforms in response to loads. Two of the most commonly required properties are the elastic modulus and Poisson's ratio (Currey, 2002). The elastic, or Young's, modulus ( $E$ ) is defined as stress/strain ( $\sigma/\epsilon$ ) measured in simple extension or compression. It is a measure of how much a material deforms under a given axial load; in other words, a numerical description of its stiffness. For example, rubber will deform far more than steel under a given load and it has a correspondingly lower  $E$ . Poisson's ratio ( $\nu$ ) is the lateral strain divided by axial strain, thus representing how much the sides of a material will contract as it is tensed (or, conversely, how the material will expand as it is compressed) to maintain volume.

One of the strengths of FEA is the ability to incorporate elastic property data into the model, but doing so accurately can also pose major challenges. In the simplest case, the material may be isotropic, meaning that it responds to load in the same manner regardless of the direction in which the load is applied. In this case, only two material constants, the elastic modulus and Poisson's ratio, are needed to describe the material. However, like many other biological structures, bone tissue is anisotropic, meaning that elastic properties vary with orientation (Currey, 2002). Cortical bone is known to have a higher elastic modulus (i.e., is stiffer) in the axial (long) direction compared to radial (perpendicular to the surface) or tangential (parallel to the surface) orientations (Reilly and Burstein, 1975). The elastic modulus in most cortical bone approximates orthotropy, which is a type of anisotropy in which the internal structure of the material creates unique elastic properties along each of the three orthogonal axes of the material (three elastic and shear moduli and six Poisson's ratios).

The most general anisotropic description of a material requires 21 independent elastic coefficients, but this degree of complexity is rarely warranted. In orthotropic materials, this complexity is reduced to nine independent elastic coefficients. In most studies of postcranial bone, the complexity is further reduced to five independent elastic coefficients by considering the structure of the bone to approximate transverse isotropy, in which elastic properties are identical in the tangential and circumferential orientations in cortical bone. However, this simplification is often unwarranted in cranial cortical bone (Peterson and Dechow, 2003; Schwartz-Dabney and Dechow, 2003).

Other more complex material properties may be modeled as well, such as nonlinear elasticity and viscoelasticity in which deformation varies nonlinearly with loading or with the rate of loading, as is the case when bones or other tissues are loaded to the extent that they undergo plastic deformation and ultimately failure. However, in most investigations of structural biomechanics, bone is treated as a linearly elastic material based on its elastic properties in response to physiologically normal loads.

Modeling the elastic properties of bone can be further complicated by the fact that mechanical properties may vary within and between bones of an individual (Yamada and Evans, 1970; Papadimitriou et al., 1996; Peterson and Dechow, 2003). For example, cortical bone elastic properties vary throughout a single skull (Peterson and Dechow, 2003) or mandible (Schwartz-Dabney and Dechow, 2003). Further, there can be considerable interindividual variation in the cortical bone of some regions of the cranial skeleton (Peterson and Dechow, 2003). These variations present a formidable modeling challenge. At one extreme, every element could have its own elastic properties corresponding to its geometric position on the skull. This approach would be prohibitively time-consuming in terms of modeling (and require comprehensive data on material property variation) and may not increase the accuracy of the model in proportion to the effort. The other, simpler and more common extreme is to ignore the variation and model all the elements as having the same elastic properties. Even this simple approach can be complicated in the skull by the fact that cranial cortical bone is orthotropic, but the orientations of the material axes do not align relative to anatomical axes.

Generally, the radial material axis of orthotropic cortical bone in long bone is considered to be exactly perpendicular to the bone surface while the other two are parallel to it; the longitudinal axis is considered to be parallel with the long axis of the bone, while the circumferential axis is perpendicular to it and oriented in the direction of the curvature of the cortex (around the circumference of the shaft of a long bone). However, there is actually little direct evidence for this configuration, and it does not hold true for the cortex of cranial bones, in which it is often difficult to define relative to an anatomically longitudinal skeletal axis (Peterson and Dechow, 2003; Schwartz-Dabney and Dechow, 2003). Recent work in one of our laboratories (Chung and Dechow, 2003 and data not shown) suggests that bulk cortical cranial bone in most regions of the mandible and facial skeleton, but not in the cranial vault, is approximated by an orthotropic structure, and the radial axis is indeed usually perpendicular to the plane of the cortical plate.

This orthotropic structure can create considerable problems when attempting to create accurate FE models. In FE modeling software, the elastic properties are typically defined relative to the global axes of the entire model (e.g.,  $x$ ,  $y$ , and  $z$  representing anatomical or some other predefined axes). However, the orientations of actual material axes do not necessarily correspond with any single Cartesian or global reference frame, but rather vary with the curvature of the bones. This makes it difficult to assign empirical elastic properties into a global reference frame if the bone shape is highly curved, as it is in most part of the craniofacial skeleton. Researchers also face the challenge of modeling differences in elastic properties in different tissue types, such as skull sutures or cancellous bone

regions (Herring and Teng, 2000). More research is needed to assess the impact of various simplifications of the complex variation found in the elastic properties of some skeletal elements on the reliability of associated FE models. Initial studies by our group (Strait et al., 2005, this issue) found that incorporating variation in elastic properties across regions of the skull significantly improved the validation of a cranial FE model against experimental data.

After the elastic properties are defined, the elements are assembled into a global stiffness matrix  $[K]$ . Here the connections between elements and nodes are defined within the model's global framework in the form of  $\{F\} = [K]\{D\}$ . The geometry of each element is completely described by the list of nodes of which it is comprised and this is referred to as the element connectivity (Hart, 1989). The element coordinate system (x-, y-, and z-coordinates of each element) is defined relative to a global frame of reference (X-, Y-, and Z-axes of the entire model).

### Boundary Conditions

There are two types of boundary conditions. The kinematic or essential boundary conditions (see Appendix) are displacement constraints that prevent rigid movement of the model; the boundary constraints in effect anchor the model. The natural or nonessential boundary conditions include the loading conditions (e.g., forces) applied to the model. Some researchers use the term "boundary conditions" to refer specifically to the essential constraints. We refer to these essential boundary conditions as boundary or displacement constraints, and the nonessential ones as loading conditions.

Boundary constraints are necessary because although the external forces may be carefully calculated such that the model should be in equilibrium, it is virtually impossible to ensure that the forces are in perfect equilibrium (i.e., vectors collectively sum to zero) when applied to the model. If the forces were not in perfect equilibrium, the model would "move." Moreover, without boundary constraints, there are an infinite number of solutions to the problem. The entire model can be uniformly displaced (moved) in the frame of reference as a rigid body without affecting the elastic response of the structure. Therefore, the boundary constraints anchor the model and enable a unique elasticity solution to be obtained. Without boundary constraints, the FE computations will not be possible.

The boundary constraints may have a significant impact on model solution and must be chosen carefully. For example, nodes at one or more locations of ligament attachment sites might be selected as the location(s) to constrain the model from translation or rotation (Richmond, 1998). One might constrain nodes at the location of a reaction force (e.g., the bite point) rather than input an estimated reaction force (e.g., resulting from the masticatory muscle forces). This will in effect apply the necessary reaction force at that location.

Depending on the element types, specific nodes may be modeled with any combination of constraints from translation in, or rotation about, any axis direction (x, y, and z). Thus, constraints include six possible variables, although solid elements typically only allow translational constraints (these elements do not have rotational degrees of freedom). At a minimum, the model must be constrained in some manner from translation in all three directions. Three-dimensional models must have sufficient boundary

constraints to prevent all six possible modes of rigid body motion. Although it is possible to constrain the entire model at a few nodes, this typically results in an unrealistic condition in which very high strains and stresses are localized around the constrained node. In general, constraints should be placed away from the primary region of interest because of potential local effects. Slight inaccuracies in modeling the constraints are likely to influence the strains and stresses adjacent to the constraints, but have little to no effect on regions more distant to the constrained nodes (Cook et al., 2001).

Functional morphologists are often interested in how a structure behaves under specific loading conditions. Several factors are important in defining the loading conditions. The forces in the model are vectors and therefore have points of application, magnitudes, and directions. The location of the loads (e.g., muscle force) may be approximated based on the researcher's knowledge of the anatomical region or defined more precisely using location measurements taken from images or during dissections. For example, the temporalis muscle could be modeled as originating from the entire cranial surface within the temporal line or more precisely measured using a 3D digitizer.

The direction of the loads can be more challenging to model. In the case of muscles, one might approximate the 3D direction of the entire muscle from its origin to its insertion. For example, from its origin on the lateral cranial surface, the temporalis might be modeled such that the vectors at each node are oriented in a uniformly inferior direction (Fig. 4a). This would surely be an oversimplification since the anterior temporalis fibers are directed inferiorly, whereas the posterior fibers are directed more anteriorly. One might more accurately approximate the muscle direction by modeling patches of muscle vectors that approximate the direction toward the insertion (Fig. 4b). The most accurate approach might involve measurements on a cadaver of individual muscle fibers from their origin (e.g., using a 3D digitizer in a reference frame that could be translated into the FE model's global reference) and inputting specific muscle vector directions across the temporalis origin. At some point, incremental increases in precision require disproportionately increasing effort. Further research is needed to determine the impact of different muscle modeling approaches on the accuracy of the model.

Load magnitudes must also be determined. External loads, such as a bite force or ground reaction force, might be measured and incorporated in the model. Others, such as muscle forces, can be reasonably approximated using muscle physiological cross-sectional area as a surrogate of maximum potential muscle force (Ross et al., 2005, this issue). Combining cross-sectional area with electromyographic (EMG) information on timing and relative magnitude of muscle recruitment can provide an estimate of muscle force magnitudes during the biomechanical event of interest (e.g., peak bite force, peak strain, mid support). A complication of using EMG data is the latency between EMG activity in a muscle and force production due to the time it takes for muscle tissue to contract in response to the nerve stimulation (Ross et al., 2005, this issue). Moreover, some muscles (e.g., masseter, temporalis) do not contract uniformly (Hylander and Johnson, 1994; Hylander et al., 2004). In such cases, greater accuracy might be achieved by independently modeling muscle subdivisions. As is the case with muscle orientations, further

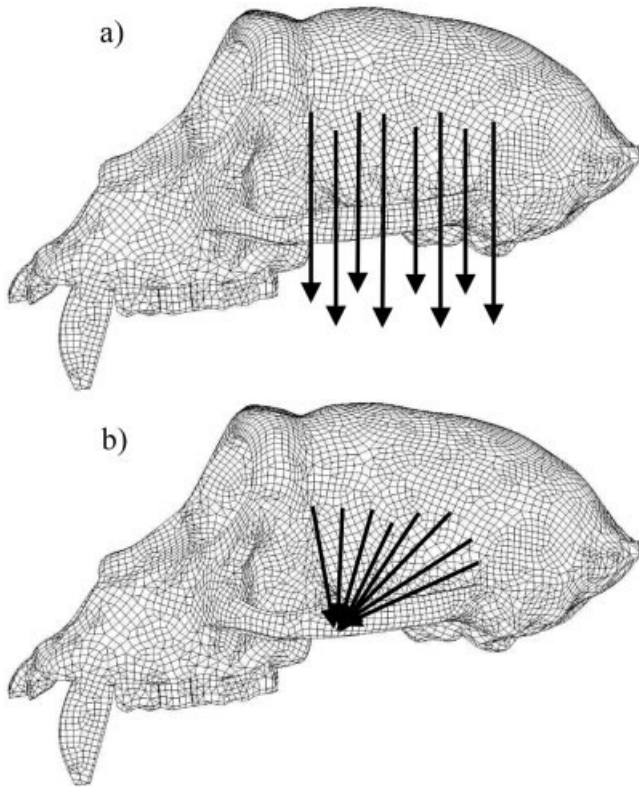


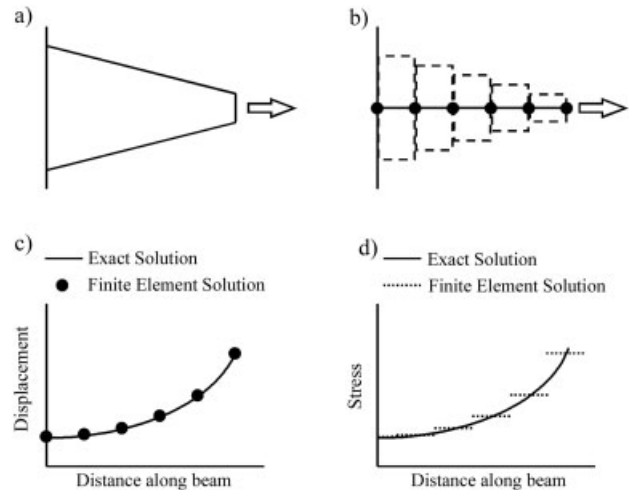
Fig. 4. Alternative ways of modeling the temporalis muscle shown on a lateral view of a macaque skull. Modeling external forces involves the identification of the locations, orientations, and magnitudes of force vectors. In **a**, the temporalis muscle is oversimplified with all vectors oriented inferiorly with the same magnitudes. In **b**, the temporalis force vectors are more realistically oriented toward the insertion on the coronoid process of the mandible. However, modeling the muscle more precisely requires information about the distribution of the muscle's origin, the orientation of force from individual muscle fibers, its degree of recruitment during an event, and the regional recruitment (e.g., anterior vs. posterior fibers) of the muscle during the event.

research is needed on muscle and other load magnitudes to assess the impact of modeling precision on the ultimate validity of the model.

**SOLUTION**

The completed model is solved to obtain the nodal displacements and then the resulting stresses and strains. The FE method approximates the exact solution through calculations at a finite number of nodes representing the structure (Fig. 5). A brief introduction to the general mathematical theory of the finite-element method is presented in the Appendix. Here, we limit our discussion to the basic principles involved in solving the FE model for the simple case of 1D bars or spring-like members.

In structural mechanics, the FE model can be envisioned as a large system of springs that deform in prescribed ways to imposed loads. The elastic modulus (*E*; stiffness) and other elastic properties determine what nodal displacements result from the nodal forces. Stress ( $\sigma = F/A$ ) and strain ( $\epsilon = \Delta L/L$ ) are related by *E* for a given elastic property as  $E = \sigma/\epsilon$ . In most biomechanical models,



(adapted from Beaupre & Carter, 1992)

Fig. 5. A simple fixed tapered beam with an axial force (**a**) can be modeled as a finite-element problem with six nodes and five 1D elements (**b**). Strain (displacements; **c**) and stress (**d**) calculated by the model approximate the exact solution. Adapted from Beaupre and Carter (1992).

the forces are known (or assumed) and the resulting stresses or strains are the data of interest. In order to determine the change in length ( $\Delta L$ ) for each element, the equation  $E = \sigma/\epsilon$  can be derived further in the following manner:

$$\sigma = E\epsilon$$

$$F/A = E(\Delta L/L)$$

$$F = \frac{EA}{L}(\Delta L)$$

Consider the 1D two-noded bar element *e* with forces  $f_1$  and  $f_2$  acting on its two nodes with nodal displacements  $u_1$  and  $u_2$  shown in Figure 6. Based on the elementary mechanics from the above equation, the stiffness of this element is given by  $E^e A^e / L^e$ . Note that the positive x-direc-

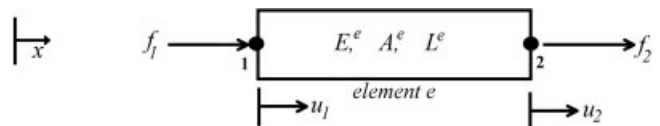


Fig. 6. Diagrammatic representation of the element equations in a simple element. Here, a 1D two-noded bar element *e* with forces  $f_1$  and  $f_2$  act on its two nodes with nodal displacements  $u_1$  and  $u_2$ . The stiffness of this element is given by  $E^e A^e / L^e$ , which includes information about the element's elastic material properties, area, and length. Note that the positive x-direction nodal force  $f_1$  is a compressive force. Its value is given by the compressive deformation of the bar,  $u_1 - u_2$ , times the bar's stiffness,  $E^e A^e / L^e$ . Similarly, the nodal force  $f_2$  is a tensile force equal to the tensile deformation of the bar,  $u_2 - u_1$ , times the bar's uniaxial stiffness,  $E^e A^e / L^e$ .

tion nodal force  $f_1$ , as illustrated in Figure 6, is a compressive force. Its value is given by the compressive deformation of the bar,  $u_1 - u_2$ , times the bar's stiffness,  $E^e A^e / L^e$ . Similarly, an assumed positive nodal force  $f_2$  is a tensile force equal to the tensile deformation of the bar,  $u_2 - u_1$ , times the bar's uniaxial stiffness,  $E^e A^e / L^e$ . Thus,

$$f_1 = \frac{E^e A^e}{L^e} (u_1 - u_2)$$

$$f_2 = \frac{E^e A^e}{L^e} (u_2 - u_1)$$

In matrix notation, the above element equations are expressed as

$$\{f\} = [K^e]\{d\}$$

$$[K^e] = \frac{E^e A^e}{L^e} \begin{bmatrix} 1 & -1 \\ -1 & 1 \end{bmatrix}$$

Due to the connection of elements together by shared nodes, the individual element equations are assembled into a set of simultaneous algebraic equations that relates all the nodal displacements to nodal forces via the system stiffness matrix:

$$\{F\} = [K]\{D\}$$

where  $\{F\}$  is the vector of nodal forces (the loads applied to the model),  $[K]$  is referred to as the system stiffness matrix because it contains information about elastic properties and geometry, and  $\{D\}$  is the vector of nodal displacements (i.e., the  $\Delta L$  values). Therefore, the external forces  $\{F\}$  and mechanical properties and geometry  $[K]$  are used to calculate the displacements  $\{D\}$  at each node (Cook et al., 2001). Once nodal displacements are known, the displacement field is interpolated from nodal values using standard interpolating polynomial functions. If the element is linear, then the interpolating polynomial is linear. Differentiation of the displacement field yields the strain distribution. The stress distribution is then obtained using the elastic property or constitutive relations (e.g.,  $E = \sigma/\epsilon$ ), which relate strains ( $\epsilon$ ) to stresses ( $\sigma$ ).

In the FE method, the theoretically exact stress tensor in equilibrium equations is replaced with an approximate one (the FEM stress tensor), resulting in a residual or error function that is a function of spatial coordinates and unknown parameters in our FEA formulation (nodal degrees of freedom). Similarly, boundary equilibrium equations are no longer satisfied when an approximate solution is used, yielding a boundary residual or error function. Using a mathematical approach known as Galerkin's method of weighted residuals (see Appendix), the FEM forces the domain and boundary residual functions to be zero (orthogonal to the weighting functions; see Appendix for more details). With this approach, as the mesh is refined, the error functions must come closer and closer to the zero function. Since only the exact solution completely satisfies the domain and boundary equilibrium equations, the finite-element solution must converge to the theoretic

cal exact solution. This approach ensures that the discretization error (the error involved in replacing a continuous structure with a finite number of elements) can be reliably decreased with increasing element density. In other words, as the number of nodes increases, the precision of the model increases. Empirically, the approximations tend to match closely the exact solution when it can be calculated (Fig. 5).

## VALIDATION AND INTERPRETATION

No matter how much thought and research goes into model creation, the results may be wrong. For biological problems, researchers should be able to address both the precision and accuracy of the model (Huiskes and Chao, 1983). Accuracy is defined here as the closeness of the model's results to the real biological situation. Precision is defined here as the closeness of the model's results to the exact solution of that biomechanical model. Various terms are used in the literature to describe these types of validity. Our definitions of the terms "accuracy" and "precision" reflect their use in statistics and other fields, but correspond with Huiskes and Chao's (1983) terms "validity" and "accuracy," respectively.

In this sense, precision is similar to its use in statistics, where it relates to the number of significant figures recorded for measurements (Sokal and Rohlf, 1995). A model would be precise but inaccurate if the mesh is very dense but the loading and boundary conditions are unrealistic. Precision and accuracy require different kinds of validation.

The precision of a particular FE model can be assessed through a convergence test in which the model is repeatedly calculated with increasingly finer meshes until the displacement magnitude of a chosen test area reaches a plateau, converging toward a precise solution of that model (Hart, 1989). In the past, assessing precision was an important step because limitations on computer power required researchers to determine an appropriate degree of mesh refinement that was reasonably precise but minimized computational demand. This has become less of an issue with more powerful computers that allow programs automatically to generate meshes that typically have ample density and increase mesh density in regions likely to undergo high stress concentrations. However, the only way to assess discretization error is to conduct a convergence test in which specific analytic quantities (e.g., maximum principal strain) at specific locations are compared between three or more meshes of different refinement.

No matter how finely the structure is meshed and how precisely the calculations are performed, the computed answer may still be wrong (Cook et al., 2001). Independent experimental support is critical to any FEA attempting to model a mechanical problem in a realistic manner. The best means of validation involves the direct measurement of strain, as in *in vivo* strain gauge experiments (Rubin and Lanyon, 1982; Hylander and Johnson, 1992; Ross, 2001). Cadaver strain experiments are also useful and provide greater control over biomechanical variables (Ross and Hylander, 1996; Richmond, 1998). A combination of *in vitro* and *in vivo* experimentation potentially offers the best validation. *In vitro* validation allows one to carefully control the loads and boundary constraints in order to assess the validity of the model's geometry and elastic properties. Here, the controlled loading and boundary conditions can be put in the FE model and the FE

results compared to the *in vitro* results. If necessary, the model geometry and elastic properties can be altered to minimize the discrepancies between the model and empirical results. Once the geometry and elastic properties are adequately modeled, discrepancies between the model and *in vivo* results can be confidently attributed to the model's loads and boundary constraints, and these can be refined if the model does not accurately reflect the *in vivo* condition.

Working from the other side of the analysis, experimental work to determine the loading conditions and mechanical properties prior to modeling can also greatly improve the model. While this cannot be considered validation, empirical data put into the model from the outset can greatly improve the model's accuracy.

As in other FE modeling steps, several issues complicate the validation process. For example, the model and experimental data differ in some ways that affect attempts at validation. Published experimental data typically consist of peak strain values for a number of anatomical regions (Hylander and Johnson, 1997), although these regions may not experience peak strain simultaneously (Hylander and Johnson, 1994; Ross, 2001). However, strains occur simultaneously in static FE models. A second example concerns the fact that *in vivo* strain gauges measure strain only in the plane of the gauge. Thus, the 3D strain orientations in the FE model must be projected into the plane of the gauge in order to compare them. A third complication is that published *in vivo* strain gauge locations are unfortunately not reported with the precision necessary to make precise location comparisons between the model and the experimental subjects. In regions of high strain gradients such as the curved browridge, slight differences in location can make a large difference in strain magnitude and orientation. Greater precision in reporting anatomical locations of gauges during *in vivo* strain experiments would be an improvement. A final issue, and probably the most difficult one, is the question over the level of correspondence between the model and the *in vivo* evidence that must be reached before the model can be considered valid. The answer depends on the hypotheses and goals of the study. Some may require accuracy in absolute strain values, while others may only require that the model deforms in a broadly similar way to the real biological structure.

Some researchers have taken the approach of building abstract representations of a structure (Witzel and Preuschoft, 1999; Jenkins et al., 2002; Witzel et al., 2004). Here, researchers are attempting to model, in a traditional sense of the term, a complex system as a simplified abstraction. This approach has its merits. If successful, much can be learned about the biomechanical problem in a straightforward manner. However, researchers must be very careful to consider the limits of a simplified model if they intend to make adaptive or behavioral inferences from the model's results. Validation of the positive and negative aspects of such a model can sometimes be formulated through creative experimentation. Without such attempts at validation, it is often difficult to evaluate whether the results have any significance in the real world. Unfortunately, most FEA studies to date in functional morphology literature or in the large clinical FEA literature include little or no validation of their models (Spears and Crompton, 1996; Spears and Macho, 1998; Macho and Spears, 1999; Witzel and Preuschoft, 1999;

Rayfield et al., 2001; Witzel et al., 2004; Ryan and van Rietbergen, 2005).

Validation and model refinement can be repeated until the two converge. Near perfect validity can become very expensive in use of time and resources and may be excessive depending on the question of interest. An FE model is, after all, a model. The researcher must decide how accurate is accurate enough, but should have some evidence on which to base this decision.

After validating the model, the researcher may begin to interpret the results. As in any study, the results should obviously be interpreted in the context of the questions forming the bases of the analysis. The vast quantities of data generated in an FEA pose challenges at this stage. Visualizing the results is an almost universal first step. Beyond this step are many strategies for illustrating and evaluating the results and assessing their statistical significance. Examples can be found in the literature (e.g., Ross et al., 2005, this issue) and are beyond the scope of this review.

## APPLICATIONS

There are at least three general applications of FEA in functional morphology today. One is to develop realistic models of biological problems. This is the traditional approach in biomechanics and orthopedics, in which individual skeletal elements or joints, such as the proximal femur (Beaupre et al., 1990) or skull (Strait et al., 2005), are modeled to better understand how the bones involved behave in response to applied loads. Independent validation is most important in this kind of FEA.

Another, less frequent, use for FEA involves integrating information from multiple strain gauges to estimate shear strains in a particular cross-section. When three or more rosette gauges record strain around the circumference of a long bone, Rybicki et al.'s (1977) method can be used to estimate the position of the neutral axis of bending, the distribution of strain due to bending throughout the cross-section, and maximum strain values in compression and tension (Carter et al., 1981; Gross et al., 1992; Roszek et al., 1993; Demes et al., 1998). However, in order to calculate shear strain, simplifying assumptions or FEA are necessary (Fritton and Rubin, 2001).

A third category of applications for FEA in functional morphology is a comparative one. FEA may be used to compare the mechanical behavior of different skeletal designs of the same structure (Richmond, 1998; Ryan and van Rietbergen, 2005). In this way, FEA promises to be a powerful new tool for testing biomechanical hypotheses in extant and fossil taxa. Under similar loading conditions, the probable strain regime of a unique fossil shape may be compared to other fossil forms or related living forms. In this kind of analysis, it is important to have a good understanding of the biomechanics of the problem in living forms that are most closely related to the fossil taxa (Rudwick, 1964; Lauder, 1995). If all related living taxa share a similar biomechanical regime (e.g., same suite of muscles, attached in similar places), it is most likely that the fossil taxa did so too, despite differences in morphology. In some cases, particularly those involving extinct taxa, it may not be possible to collect some of the data that would improve the model's accuracy. In these situations, FEA can be useful if the purpose of the analysis is not absolute accuracy but the relative abilities of structures to resist loading regimes.

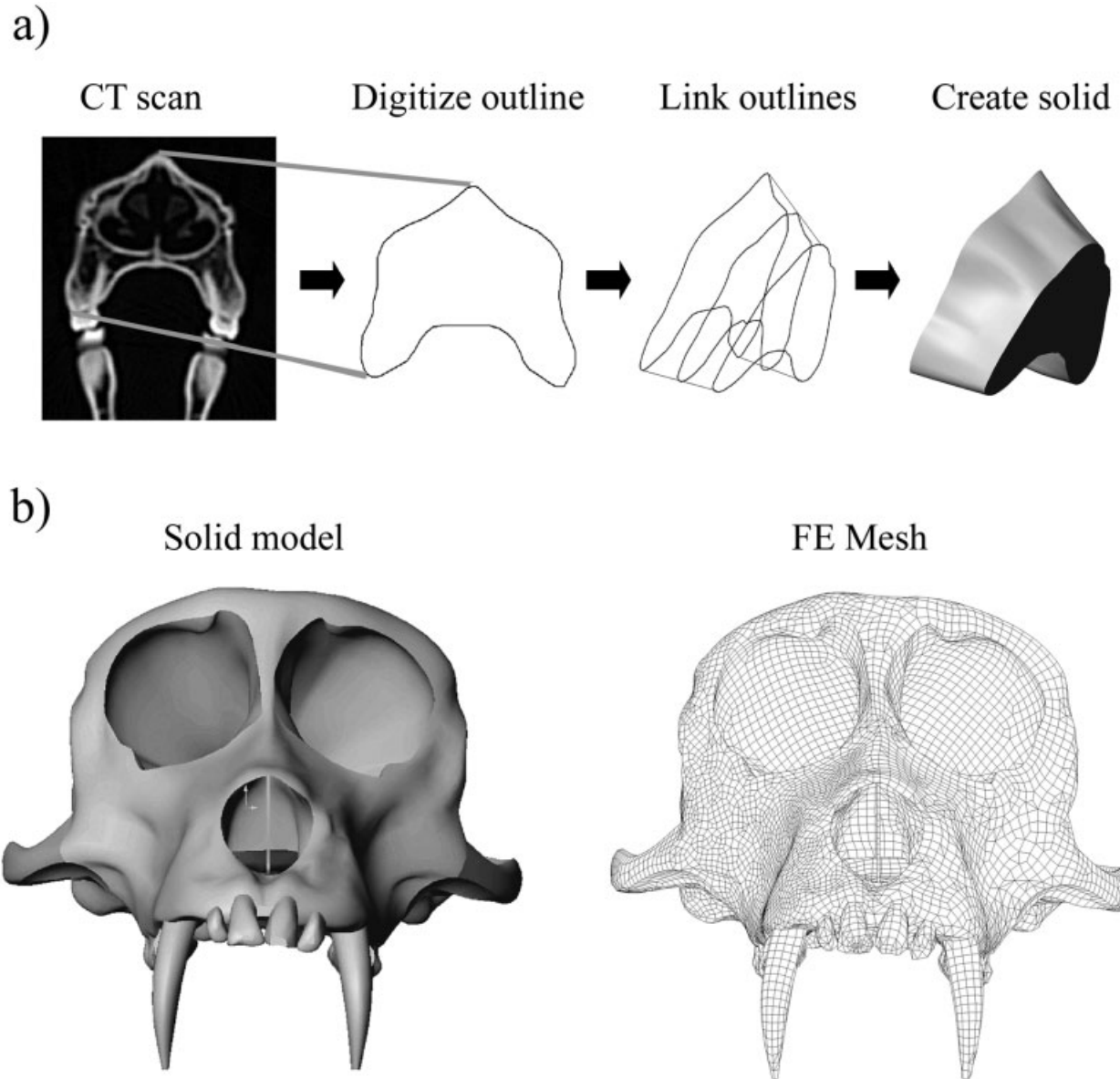


Fig. 7. An illustrative example of creating an FE mesh. **a:** The external then internal outlines of successive CT scans of a macaque skull were digitized and linked using CAD software. The linked outlines were converted into a solid CAD model. **b:** The entire solid model of a macaque skull was converted into a 3D FE mesh of linear brick and other polyhedral elements.

FEA can also be used to examine the structural behavior of specific anatomical features, such as the zygomatic arch (Witzel et al., 2004) or palate thickness (Strait et al., 2005). FE methods provide controlled experimental conditions that allow researchers to isolate the mechanical significance of a single morphological trait by comparing two organisms that differ only in that trait. FEA promises to offer new insights into the mechanical significance of novel evolutionary structures, such as the hard palate, postorbital bar, and sutural fusion in the mandible and cranial bones. FEA also offers researchers a unique way to examine the interactive mechanical effect of combinations of features not present in extant or fossil taxa. Such an

approach might allow researchers to evaluate more accurately whether features in fossil taxa should be considered as adaptations to particular functions.

An exciting new direction involves using FEA to investigate biological processes. In a pioneering example of this approach, Beaupre et al. (1990) tested their remodeling theory (e.g., the rules governing the remodeling process) by comparing real bone structure to the results of an FE model that was repeatedly loaded and altered following the rules of the theory. In this way, they were able to assess the utility of the remodeling theory and show that similar stress-related phenomena might be responsible for normal bone morphogenesis as well as functional adapta-

tion in response to altered loads (Beaupre et al., 1990). In this issue, Preuschoft and Witzel (2005), use FE modeling in a creative way to test hypotheses about potential evolutionary rules underlying skull morphology by applying muscle loads to a block with only minimal skull form (orbits, dental arcade, muscle origin locations) and comparing the resulting stress distributions against real skull form. By iteratively removing low stress regions of the block, they find that the reduced model is similar to the true skull form. These results have interesting implications for the role of optimality in the evolution of skeletal morphology. Iterative approaches like these promise to help elucidate the processes underlying the functional adaptation and morphogenesis of biological tissues and potentially the evolutionary changes in morphology in response to changes in lifestyle.

The case study below provides one example of how FE modeling can be used to investigate specific adaptive hypotheses in fossil taxa.

### CASE STUDY

The human fossil record includes an impressive diversity in craniofacial morphology (Stringer and Trinkaus, 1981; Rak, 1983; Walker et al., 1986; Brunet et al., 2002; Brown et al., 2004; Kimbel et al., 2004). Not surprisingly, these fossils have generated much discussion about craniofacial adaptations to biting and chewing. One fossil group in particular, the robust australopiths, displays a suite of derived craniofacial features and very large, thickly enameled molars and premolars (Grine, 1988). Researchers disagree on the specific suites of derived traits that they would consider adaptations to chewing, a disagreement that affects the reconstruction of their phylogenetic relationships (e.g., different suites of integrated traits) and paleobiology (Skelton and McHenry, 1998; Strait and Grine, 1998).

Our work on FE modeling of a macaque skull is aimed at building accurate primate skull models to test functional and evolutionary hypotheses and ultimately biomechanical hypotheses in fossil primate skulls. To help illustrate how FE modeling can be used to test such hypotheses, we examined the biomechanical significance of one trait, palate thickness, hypothesized to be an adaptation in robust australopithecines to increased masticatory stresses (Strait et al., 2005). We built a 3D model of a macaque skull during static centric occlusion, validated it against in vivo bone strain data, and altered the palate thickness of the model to assess the mechanical significance of this feature. We outline the FE modeling process below.

### Geometry and Mesh

The complexity of the skull and decision to compare strain at various points throughout the skulls of thick- and thin-palate FE models required a 3D model. We selected *Macaca fascicularis* because of the in vivo strain data available for this taxon (Hylander et al., 1991a; Hylander and Johnson, 1997). We obtained CT scans of the skull and manually digitized the scans in Solidworks CAD modeling software to create a virtual solid model including external and internal surfaces (Fig. 7). The models were aligned such that the occlusal plane was horizontal. The CAD wire-frame model was then imported into the FEA software ALGOR, and the automated 3D mesh-generating feature was used to cre-

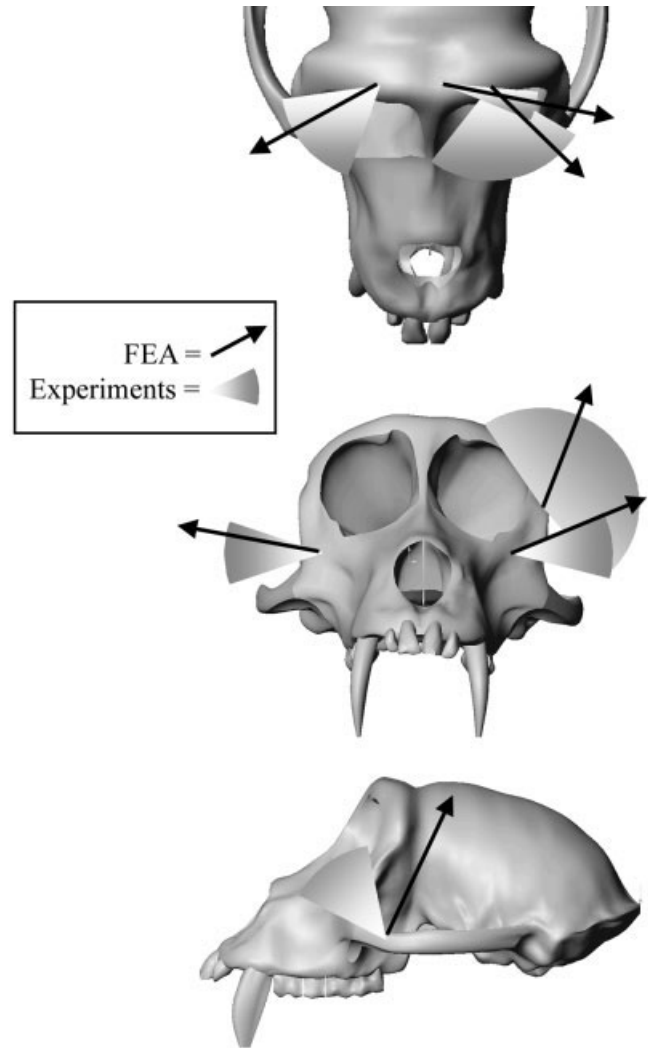


Fig. 8. The maximum principal strain orientations (and magnitudes; not shown) of the model are compared to the range of values observed from in vivo experiments of different macaque individuals. In six of the seven locations, the strain orientations lie within or adjacent to the in vivo results, indicating that the model is reasonably valid in its representation of the manner of deformation. Note that the location in which the model and experimental orientations differ is the highly curved zygomatic arch (working side). The steep strain gradients in this region leave open the possibility that some of the discrepancy might be attributable to between-individual morphological variation or lack of precision in identifying gauge location on the model. Model refinement and increased precision in measuring gauge location during in vivo experiments therefore might focus on this region.

ate an FE mesh consisting of 145,480 polyhedral brick elements (the Normal Model). We then altered the initial CAD model by artificially increasing the thickness of the palate and converted it into a second FE mesh (Thick Model) consisting of 290,639 elements. A structure as geometrically complex as the skull requires the automatic mesh-generating software to make many decisions about local mesh densities that result in different total element numbers. Although the two models differed in element number, both exhibited high concen-

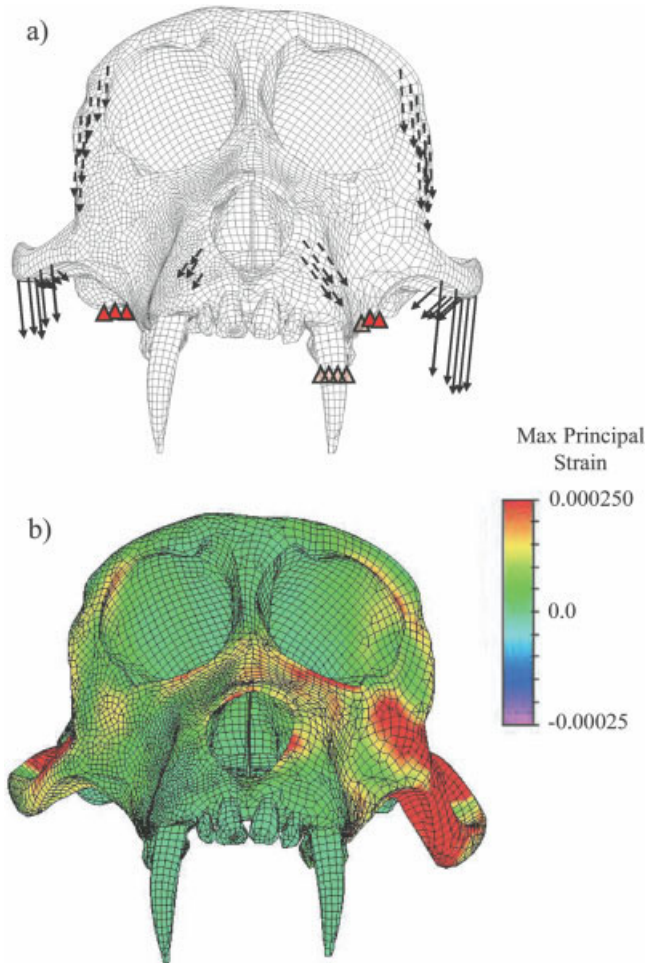


Fig. 9. Undeformed Normal Model mesh with schematic boundary conditions (a) and a meshed image (b) illustrating highly magnified deformations with maximum principal strain. Maximum principal strain shows the tensile strain magnitudes. In the undeformed model (a), solid arrows on the zygomatic arch illustrate the deep and superficial masseter muscle forces on working (macaque's left side) and balancing sides; dashed arrows illustrate the working- and balancing-side temporalis and medial pterygoid muscles behind the visible surface of the model. The arrows are not drawn to scale, but roughly illustrate the directions and relative magnitudes of the muscle (see Strait et al. 2005, in this issue for more details). Transparent triangles show the fixed nodes on the left first molar (behind the canine) and the nodes permitting rotation but not translation at the glenoid fossa. The deformed model (b) shows inferior deformation of the zygomatic arches and the superior deformation of the working side of the face due to the bite reaction force. The orbits are both pulled inferolaterally, but in an asymmetric manner because of asymmetric muscle forces and the working-side bite point. The working side maxilla (e.g., near the nasal aperture and zygomatic arch) and orbit undergo more, and qualitatively different, deformation compared to the balancing side.

trations of elements in regions that are likely to experience high strain gradients, and independent experimental data support the validity of the Normal Model.

### Material Properties

Elastic property data from 25 locations on macaque skulls were used (data not shown). As a simplification,

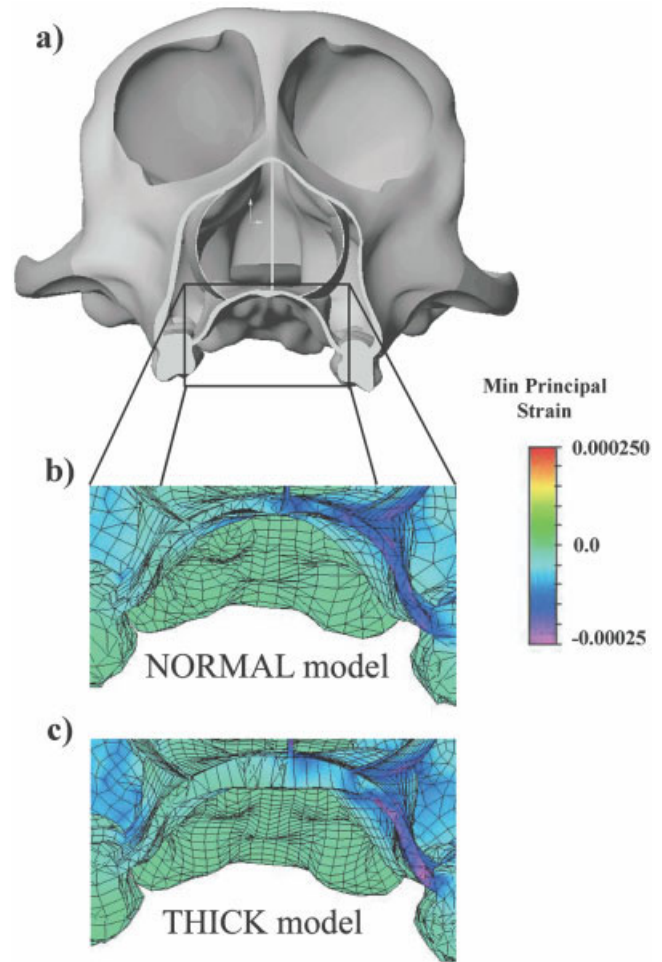


Fig. 10. The solid model (a) illustrating the location along the face where minimum principal strains are shown for the Normal Model (b) and Thick-palate Model (c). Note that compared to the Normal Model (b), strains in the Thick Model are lower in the palate itself, but are higher in some adjacent regions. This supports the hypothesis that palate thickness may be functionally related to resisting masticatory strains, but also indicates that multiple features must be integrated to serve this purpose. FE modeling methods allow researchers to assess the mechanical significance of features like these in isolation or in combination.

bone was modeled isotropically, with the values of Young's modulus (19.8 GPa) and Poisson's ratio (0.315) representing averages of the respective values in the axis of maximum stiffness obtained at all locations on the face. In a subsequent analysis, we modeled anisotropic elastic properties and properties in different regions (Strait et al., 2005, this issue).

### Boundary Conditions

The necessary boundary conditions included muscle forces and external constraints to restrict translation and rotation of the model. Eight muscle forces were applied to the meshes corresponding to the primary jaw adducting muscles: right and left anterior temporalis, superficial masseter, deep masseter, and medial pterygoid muscles. Muscle orientations were estimated by measuring the po-

sitions of muscle attachments and by examining muscle maps constructed from dissected specimens (Anton, 1999). Muscle forces were estimated by combining data on physiological cross-section and on muscle activity. By assuming that muscle force is proportional to the magnitude of muscle activity obtained from EMG studies of macaque mastication (Ross et al., 2005, this issue), the relative force magnitudes exerted by each muscle at or near centric occlusion were calculated. Root mean square (r.m.s.) EMG activity of jaw adductors precedes the force generated by those muscles by approximately 20 msec (Hylander and Johnson, 1989; Ross et al., 2005, this issue). Consequently, muscle force magnitudes were calculated as  $F = \text{cross-sectional area} \times 300 \text{ kN/m}^2 \times \% \text{ of peak activity } 20 \text{ msec prior to peak corpus strain}$ .

Two sets of boundary constraints were applied to the FE model: the articular eminences were not permitted to translate but could rotate in place, and nodes on the crown of M1 could neither translate nor rotate. This acts to pull the skull down onto the bite point, which describes how the skull experiences masticatory forces. The bite point is treated as a reaction force, similar to the real biological situation. With these elastic properties, boundary constraints, and loading conditions in place, the FE model was calculated.

### Validation

The strains in the Normal (thin-palate) Model were compared to strain magnitudes and orientations obtained from published and unpublished chewing experiments (Hylander et al., 1991b; Hylander and Johnson, 1997; Ross, 2001; Ross et al., 2002). Most strain orientations in the Normal Model were within or very near the observed variation in experimental values, indicating that the model's manner of deformation (e.g., where it experienced tension versus compression) was broadly similar to that observed in vivo (Fig. 8). Similarly, most strain magnitudes in the Normal Model compared well with those observed in vivo (Strait et al., 2005). Some of the discrepancy is almost certainly due to the imperfect resolution of the modeling assumptions. However, some of the discrepancy may also be due to differences in geometry between the in vivo subjects and the macaque used to create the model. The worst correspondence between the model and in vivo maximum principal strain orientation occurred on the working-side zygomatic arch (Fig. 8). This region is highly curved rostrocaudally and superoinferiorly, and the relatively high strain gradients (Fig. 8) in this region make it more difficult to compare data between individuals (model and experiments) that slightly differ in morphology, especially when strain gauge locations are not precisely known. For the purposes of assessing the mechanical significance of relative palate thickness, the model was considered valid based on the generally good correspondence between the model and in vivo data.

### Interpretation

The deformations show the face experiencing a complex pattern of strain (Fig. 9). The working-side zygomatic arch deforms more than the balancing-side arch as a result of the greater working-side muscle force and the proximity of the bite point preventing the working-side face from deforming inferiorly (Fig. 9). The orbits are pulled inferiorly,

tending to stretch them into a more oval shape with tension along the inferomedial and superolateral margins (Fig. 9). The working-side maxilla (e.g., near the nasal aperture, adjacent to the zygomatic arch) and orbit undergo more deformation, and in a somewhat different manner, than those of the balancing side probably as a result of the bite point location.

Compared to the Normal Model, strains in the Thick-palate Model were lower within the palate but higher in most other facial regions, particularly in the circumorbital regions and working-side zygomatic arch (Fig. 10). The only nonpalate regions that experienced reduced shear were on the sides of the rostrum, including the buccal surface of the alveolar region. These results show that palate thickness clearly affects strain patterns. However, the results also suggest that a thick palate would not have evolved in isolation as an adaptation to withstand masticatory stresses, because strain becomes elevated elsewhere. These results therefore support hypotheses that multiple features are integrated to share a stress-resistance function in taxa, such as the robust australopiths, with mechanically demanding diets. Future work will involve modeling other hypothesized masticatory features to assess their impact on the skull's strain distribution and magnitude as well as modeling combinations of features to assess hypotheses about functional integration.

### CONCLUSION

FE modeling has reached a level of sophistication and accessibility that makes it a powerful and useful tool to help refine and test biomechanical hypotheses in studies of vertebrate morphology, including fossil vertebrates. FE modeling consists of three basic steps: model creation, solution, and validation. Without validation, the model's biological relevance cannot be evaluated. In addition to its conventional use in modeling realistic biological situations, FEA can be used in a comparative experimental manner to isolate and assess the mechanical significance of individual features or combinations of features.

### ACKNOWLEDGMENTS

The workshop at which this paper was originally presented was made possible by generous funding from the International Society of Vertebrate Morphologists, *The Anatomical Record*, and the Department of Organismal Biology and Anatomy at the University of Chicago. The authors appreciate the helpful comments of Paul Constantino, Nicole Griffin, Matt Skinner, and the referees. Supported by grants from National Science Foundation Physical Anthropology SBR 9624726 (to W.L. Jungers and B.G.R.) and BCS 0240865 (to D.S.S., P.C.D., B.G.R., C.F.R., and M.A.S.).

### LITERATURE CITED

- Anton SC. 1999. Macaque masseter muscle: internal architecture, fiber length, and cross-sectional area. *Int J Primatol* 20:441–462.
- Beaupre GS, Orr TE, Carter DR. 1990. An approach for time-dependent bone modeling and remodeling: application—a preliminary remodeling situation. *J Orthop Res* 8:662–670.
- Beaupre GS, Carter DS. 1992. Finite element analysis in biomechanics. In: Biewener AA, editor. *Biomechanics: structures and systems—a practical approach*. Oxford: IRL Press. p 149–174.
- Biewener A. 1992. *Biomechanics—structures and systems: A practical approach*. Oxford: IRL Press.

- Brown P, Sutikna T, Morwood MJ, Soejono RP, Jatmiko, Saptomo EW, Due RA. 2004. A new small-bodied hominin from the Late Pleistocene of Flores, Indonesia. *Nature* 431:1055–1061.
- Brunet M, Guy F, Pilbeam D, Mackaye HT, Likius A, Ahounta D, Beauvilain A, Blondel C, Bocherens H, Boisserie JR, De Bonis L, Coppens Y, Dejax J, Denys C, Durringer P, Eisenmann V, Fanone G, Fronty P, Geraads D, Lehmann T, Lihoreau F, Louchart A, Mahamat A, Merceron G, Mouchelin G, Otero O, Pelaez Campomanes P, Ponce De Leon M, Rage JC, Sapanet M, Schuster M, Sudre J, Tassy P, Valentin X, Vignaud P, Viriot L, Zazzo A, Zollikofer C. 2002. A new hominid from the Upper Miocene of Chad, Central Africa. *Nature* 418:145–151.
- Carter DR, Harris W, Vasu R, Carter W. 1981. The mechanical and biological response of cortical bone for in vivo strain histories. In: Cawin SC, editor. *Mechanical properties of bone*. New York: American Society of Mechanical Engineers. p 81–92.
- Chung DW, Dechow PC. 2003. Contrasts in off-axis ultrasonic velocity measurements in cortical bone from human crania and femur. *J Dent Res* 82A:1509.
- Cook RD, Malkus DS, Plesha ME, Witt RJ. 2001. *Concepts and applications of finite-element analysis*, 4 ed. New York: John Wiley and Sons.
- Courant R. 1943. Variation methods for the solution of problems of equilibrium and vibrations. *Bull Am Math Soc* 49:1–23.
- Cowin SC. 1989. *Mechanics of materials*. In: Cowin SC, editor. *Bone mechanics*. Boca Raton: CRC Press. p 15–42.
- Currey JD. 2002. *Bones: structures and mechanics*. Princeton, NJ: Princeton University Press.
- Dechow PC, Hylander WL. 2000. Elastic properties and masticatory bone stress in the macaque mandible. *Am J Phys Anthropol* 112: 553–574.
- Demes B, Stern JT, Jr, Hausman MR, Larson SG, McLeod KJ, Rubin CT. 1998. Patterns of strain in the macaque ulna during functional activity. *Am J Phys Anthropol* 106:87–100.
- Fajardo RJ, Ryan TM, Kappelman J. 2002. Assessing the accuracy of high-resolution X-ray computed tomography of primate trabecular bone by comparisons with histological sections. *Am J Phys Anthropol* 118:1–10.
- Fritton SP, Rubin CT. 2001. In vivo measurement of bone deformations using strain gages. In: Cawin SC, editor. *Bone mechanics handbook*, 2nd edition. Boca Raton: CRC Press. p 8–91.
- Grine FE. 1988. Evolutionary history of the “robust” Australopithecines: a summary and historical perspective. In: Grine FE, editor. *Evolutionary history of the “robust” australopithecines*. New York: Aldine de Gruyter. p 509–520.
- Gross TS, McLeod KJ, Rubin CT. 1992. Characterizing bone strain distributions in vivo using three triple rosette strain gages. *J Biomech* 25:1081–1087.
- Hart RT. 1989. The finite-element method. In: Cowin SC, editor. *Bone mechanics*. Boca Raton, FL: CRC Press. p 53–74.
- Herring SW, Teng S. 2000. Strain in the braincase and its sutures during function. *Am J Phys Anthropol* 112:575–593.
- Huiskes R, Chao EYS. 1983. A survey of finite-element analysis in orthopedic biomechanics: the first decade. *J Biomech* 16:385–409.
- Hylander WL. 1984. Stress and strain in the mandibular symphysis of primates: a test of competing hypotheses. *Am J Phys Anthropol* 64:1–46.
- Hylander WL, Johnson KR. 1989. The relationship between masseter force and electromyogram during mastication in the monkey *Macaca fascicularis*. *Arch Oral Biol* 34:713–722.
- Hylander WL, Johnson KR. 1992. Strain gradients in the craniofacial region of primates. In: Davidovitch Z, editor. *The biological mechanisms of tooth movement and craniofacial adaptation*. Columbus, OH: Ohio State University. p 559–569.
- Hylander WL, Johnson KR. 1994. Jaw muscle function and wishboning of the mandible during mastication in macaques and baboons. *Am J Phys Anthropol* 94:523–547.
- Hylander WL, Johnson KR. 1997. In vivo bone strain patterns in the zygomatic arch of macaques and the significance of these patterns for functional interpretations of craniofacial form. *Am J Phys Anthropol* 102:203–232.
- Hylander WL, Picq PG, Johnson KR. 1991a. Bone strain and the supraorbital region of primates. In: Carlson DS, Goldstein SA, editors. *Bone biodynamics in orthodontic and orthopedic treatment*. Ann Arbor: Center for Human Growth and Development. p 315–349.
- Hylander WL, Picq PG, Johnson KR. 1991b. Masticatory-stress hypotheses and the supraorbital region in primates. *Am J Phys Anthropol* 86:1–36.
- Hylander WL, Ravosa MJ, Ross CF. 2004. Jaw muscle recruitment patterns during mastication in anthropoids and prosimians. In: Anapol F, German RZ, Jablonski NG, editors. *Shaping primate evolution*. Cambridge: Cambridge University Press. p 229–257.
- Jenkins I, Thomason JJ, Norman DB. 2002. Primates and engineering principles: applications to craniofacial mechanisms in ancient terrestrial predators. *Senckenbergiana Lethaea* 82:223–240.
- Kappelman J. 1998. Advances in three-dimensional data acquisition and analysis. In: Strasser E, Fleagle JG, Rosenberger A, McHenry HM, editors. *Primate locomotion: recent advances*. New York: Plenum Press. p 205–222.
- Kimbel WH, Rak Y, Johanson DC. 2004. *The skull of australopithecus afarensis*. Oxford: Oxford University Press.
- Lauder GV. 1995. On the inference of function from structure. In: Thompson JJ, editor. *Functional morphology in vertebrate paleontology*. Cambridge: Cambridge University Press. p 1–18.
- Levy S. 1953. Structural analysis and influence coefficients for delta wings. *J Aero Sci* 20:805–823.
- Macho GA, Spears IR. 1999. Effects of loading on the biomechanical behavior of molars of *Homo*, *Pan*, and *Pongo*. *Am J Phys Anthropol* 109:211–227.
- Mackerle J. 1995. Some remarks on progress with finite-elements. *Comp Struct* 55:1101–1106.
- Papadimitriou HM, Swartz SM, Kunz TH. 1996. Ontogenetic and anatomic variation in mineralization of the wing skeleton of the Mexican free-tailed bat, *Tadarida brasiliensis*. *J Zool Lond* 240: 411–426.
- Pavalko FM, Norvell SM, Burr DB, Turner CH, Duncan RL, Bidwell JP. 2003. A model for mechanotransduction in bone cells: the load-bearing mechanosomes. *J Cell Biochem* 88:104–112.
- Peterson J, Dechow PC. 2003. Material properties of the human cranial vault and zygoma. *Anat Rec* 274A:785–797.
- Preuschoft H. 1970. Functional anatomy of the lower extremity. In: Bourne, editor. *The chimpanzee*, vol. 3. Basel: Karger. p 221–294.
- Preuschoft H, Witzel U. 2005. The functional shape of the skull in vertebrates: which forces determine skull morphology in lower primates and ancestral synapsids? *Anat Rec* 283A:402–413.
- Rak Y. 1983. *The australopithecine face*. New York: Academic Press.
- Rayfield EJ, Norman DB, Horner CC, Horner JR, Smith PM, Thomason JJ, Upchurch P. 2001. Cranial design and function in a large theropod dinosaur. *Nature* 409:1033–1037.
- Rayfield EJ. 2004. Cranial mechanics and feeding in *Tyrannosaurus rex*. *Proc Royal Soc Lond B Biol Sci* 271:1451–1459.
- Reilly DT, Burstein AH. 1975. The elastic and ultimate properties of compact bone tissue. *J Biomech* 8:393–405.
- Richmond BG. 1998. *Ontogeny and biomechanics of phalangeal form in primates*. PhD Dissertation. Stony Brook, NY: State University of New York. p 240.
- Ross CF, Hylander WL. 1996. In vivo and in vitro bone strain in the owl monkey circumorbital region and the function of the postorbital septum. *Am J Phys Anthropol* 101:183–215.
- Ross CF. 2001. In vivo function of the craniofacial haft: the interorbital “pillar.” *Am J Phys Anthropol* 116:108–139.
- Ross CF, Strait D, Richmond BG, Spencer MA. 2002. In vivo bone strain and finite-element modeling of the anterior root of the zygoma on *Macaca*. *Am J Phys Anthropol* 24(Suppl):200.
- Ross CF, Patel BA, Slice DE, Strait DS, Dechow PC, Richmond BG, Spencer MA. 2005. Modeling masticatory muscle force in finite-element analysis: sensitivity analysis using principal coordinates analysis. *Anat Rec* 283A:288–299.
- Rubin CT, Lanyon LE. 1982. Limb mechanics as a function of speed and gait: a study of functional strains in the radius and tibia of horse and dog. *J Exp Biol* 101:187.

- Rubin CT, Lanyon LE. 1984. Dynamic strain similarity in vertebrates: an alternative to allometric limb bone scaling. *J Theor Biol* 107:321–327.
- Rudwick MJS. 1964. The inference of function from structure in fossils. *Br J Phil Sci* 15:27–40.
- Ruff CB. 1995. Biomechanics of the hip and birth in early *Homo*. *Am J Phys Anthropol* 98:527–574.
- Ryan TM, van Rietbergen B. 2005. Mechanical significance of femoral head trabecular bone structure in *Loris* and *Galago* evaluated using micromechanical finite-element models. *Am J Phys Anthropol* 126: 82–96.
- Rybicki EF, Mills EJ. 1977. In vivo and analytical studies of forces and moments in equine long bones. *J Biomech* 10:701–705.
- Schwartz-Dabney CL, Dechow PC. 2003. Variations in cortical material properties throughout the human dentate mandible. *Am J Phys Anthropol* 120:252–277.
- Silva MJ, Brodt MD, Hucker WJ. 2005. Finite element analysis of the mouse tibia—estimating endocortical strain during three-point bending in SAMP6 osteoporotic mice. *Anat Rec* 283A:380–390.
- Skelton RR, McHenry HM. 1998. Trait list bias and a reappraisal of early hominid phylogeny. *J Hum Evol* 34:109–113.
- Sokal RR, Rohlf FJ. 1995. *Biometry*, 3rd ed. New York: W.H. Freeman.
- Spears IR, Crompton RH. 1996. The mechanical significance of the occlusal geometry of great ape molars in food breakdown. *J Hum Evol* 31:517–535.
- Spears IA, Macho GA. 1998. Biomechanical behaviour of modern human molars: implications for interpreting the fossil record. *Am J Phys Anthropol* 106:467–482.
- Strait DS, Grine FE. 1998. Trait list bias? a reply to Skelton and McHenry. *J Hum Evol* 34:115–118.
- Strait DS, Wang O, Dechow PC, Ross CF, Richmond BG, Spencer MA, Patel BA. 2005. Modeling elastic properties in finite element analysis: How much precision is needed to produce an accurate model? *Anat Rec* 283A:275–287.
- Strait DS, Richmond BG, Spencer MA, Ross CF, Dechow PC, Wood BA. Masticatory biomechanics and its relevance to early hominid phylogeny: an examination of palate thickness using finite element analysis. *J Hum Evol* (in press).
- Stringer CB, Trinkaus E. 1981. The Shanidar Neandertal crania. In: Stringer CB, editor. *Aspects of human evolution*. London: Taylor and Francis. p 129–165.
- Turner CH. 1998. Three rules for bone adaptation to mechanical stimuli. *Bone* 23:399–407.
- Walker AC, Leakey RE, Harris JM, Brown FH. 1986. 2.5-Myr *Australopithecus boisei* from west of Lake Turkana, Kenya. *Nature* 322:517–522.
- Witzel U, Preuschoft H. 1999. The bony roof of the nose in humans and other primates. *Zool Anz* 238:103–115.
- Witzel U, Preuschoft H, Sick H. 2004. The role of the zygomatic arch in the statics of the skull and its adaptive shape. *Folia Primatol* 75:202–218.
- Yamada H, Evans FG. 1970. *Strength of biological materials*. Baltimore: Williams and Wilkins.

## APPENDIX: BRIEF INTRODUCTION TO FEA THEORY FOR TWO-DIMENSIONAL ELASTICITY

A brief mathematical overview of the finite-element method is presented for the case of 2D elasticity. The extension to three dimensions is straight forward, as well as to problems governed by other differential equations of equilibrium. The reader will need a basic understanding of mechanics of materials and multivariable calculus.

### Theoretical Analysis of Elasticity Problems

At any material point in the domain, there exists a differential element of finite thickness  $t$  but differential or infinitesimal volume  $t dx dy$  (Fig. 11) in equilibrium with

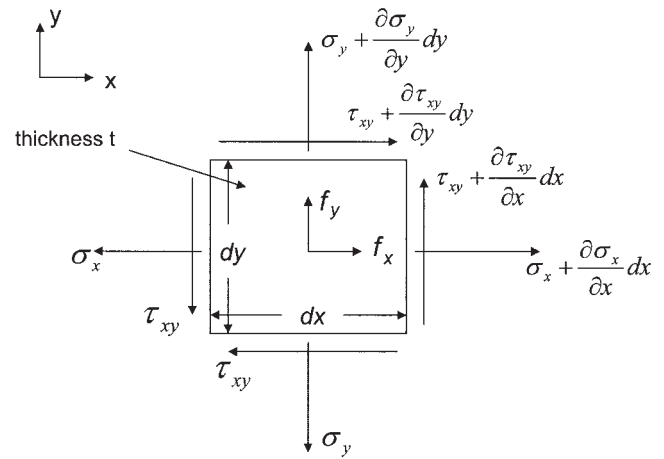


Fig. 11. Stress components and body forces that act on a differential element of volume  $t dx dy$  at a material point in the domain

the stress components and externally applied body forces that act on it. Stress components are multiplied by the surface areas they act on to yield force components. By summing forces to zero in the  $x$ - and  $y$ -directions and dividing the resulting equations by the differential volume  $t dx dy$ , one obtains the differential equations of equilibrium for 2D elasticity.

$$\begin{aligned} \frac{\partial \sigma_x}{\partial x} + \frac{\partial \tau_{xy}}{\partial y} + f_x &= 0 \\ \frac{\partial \tau_{xy}}{\partial x} + \frac{\partial \sigma_y}{\partial y} + f_y &= 0 \end{aligned} \quad x, y \in \Omega \quad (1)$$

where  $f_x$  and  $f_y$  are body forces (force/unit volume) acting on the differential element (such as due to gravity or inertia loading) and  $\Omega$  represents the volume domain. The equilibrium equations can be written more succinctly using tensor notation. In tensor notation, the differential equilibrium equations are

$$\nabla \cdot [\sigma] + \{f\} = 0 \quad x, y \in \Omega \quad (2)$$

where  $[\sigma]$  is the stress tensor and  $\nabla \cdot$  is the divergence operator.

Two types of boundary conditions are possible. On some portions of the boundary of the physical domain, displacements are specified. Prescribed or specified displacements are called kinematic or essential boundary conditions. These boundary conditions are called essential for good reason, for unless sufficient kinematic boundary conditions are imposed to prevent all possible modes of rigid body motion, a unique solution to Equation 2 does not exist. The second type of boundary condition is called natural or nonessential and is the prescription of forces or tractions (force per unit area) on the boundary. Let  $\bar{\tau}$ , denote a prescribed traction vector acting on a plane of differential length  $ds$  whose orientation is defined by the unit outward normal  $\hat{n}$ . The total applied force to this differential boundary section is  $\bar{\tau} t ds$  with components in the  $\hat{n}$  and  $\hat{t}$  directions of  $\bar{\tau}_n t ds$  and  $\bar{\tau}_t t ds$ , respectively (Fig.

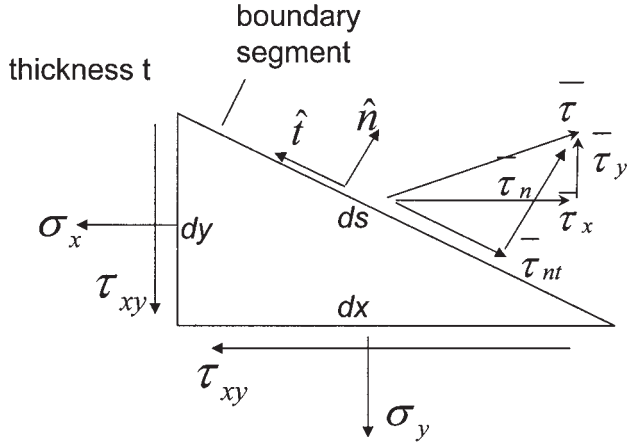


Fig. 12. Internal stress components and surface tractions that act on a differential element with boundary surface  $t ds$  at a material point on the boundary of the domain.

12). Again, Newton's laws of statics must hold, so this differential boundary wedge element must be in static equilibrium; the forces due to the externally applied traction  $\bar{\tau}$  on the boundary surface  $t ds$  must be in equilibrium with the forces due to the internal stress components. Thus, by summing forces in the  $x$ - and  $y$ -directions and after some trigonometric and algebraic manipulations, one has

$$\bar{\tau}_x - \sigma_x \hat{n}_x + \tau_{xy} \hat{n}_y = 0 \quad (3)$$

$$\bar{\tau}_y - \tau_{xy} \hat{n}_x + \sigma_y \hat{n}_y = 0 \quad (4)$$

which in tensor notation has the form

$$\{\bar{\tau}\} - \{\hat{n}\} \cdot \{\sigma\} = 0 \quad x, y \in \Gamma_n \quad (5)$$

where  $\Gamma_n$  denotes the portion of the boundary of the domain subjected to the externally applied tractions.

Equation 2 is a first-order differential equations in terms of the unknown stress tensor  $\{\sigma\}$ . Material property relationships (see text) relate the stress tensor to the strain tensor through experimentally determined material properties. Strains, in turn, are related to displacements through known differential strain-displacement relations. For example, for a 1D elasticity problem  $\epsilon_x = du/dx$ , where  $u$  is the displacement in the  $x$ -direction and  $\epsilon_x$  is the strain in the  $x$ -direction. Thus, by exploiting the material property relationships and strain-displacement relations, Equation 2 can be transformed into second-order partial differential equations in terms of the  $x$  and  $y$  displacement fields  $u = u(x, y)$  and  $v = v(x, y)$ , respectively. Thus, to solve Equation 2 for the exact displacement fields  $u(x, y)$  and  $v(x, y)$ , it must be integrated twice and the proper boundary conditions applied. The exact displacement fields are then differentiated to yield the exact strain tensor throughout the domain, and the exact stresses throughout the domain are found through the known stress-strain relationships. Unfortunately, in the real world, physical domains  $\Omega$  are typically irregular in

shape (especially for biological systems), material properties may vary spatially, multiple types of materials may exist in the domain, material relationships may be complex, such as anisotropic, viscoelastic, hyperelastic, etc., and all types of loading conditions and constraints may exist. Thus, theoretically exact solutions to elasticity problems exist for only the simplest or mostly highly idealized problems.

### Finite-Element Analysis of Elasticity Problems

In the finite-element method, an approximate solution,  $\bar{u}(x, y)$  and  $\bar{v}(x, y)$ , to the elasticity problem is sought, which results in approximate strain and stress tensors  $\{\bar{\epsilon}\}$  and  $\{\bar{\sigma}\}$ . It turns out that it is relatively straightforward to construct an approximate solution that satisfies all the kinematic boundary conditions exactly. However, when the approximate solution is substituted into both the domain differential equilibrium equations represented by Equation 2 or the boundary differential equilibrium equations represented by Equation 5, equilibrium is not satisfied exactly. This lack of satisfaction of differential equilibrium is reflected in a domain and boundary residual (i.e., error) vector functions given by

$$\{R_\Omega(x, y)\} = \nabla \cdot \{\bar{\sigma}\} + \{f\} = \left\{ \begin{array}{l} \frac{\partial \bar{\sigma}_x}{\partial x} + \frac{\partial \bar{\tau}_{xy}}{\partial y} + f_x \\ \frac{\partial \bar{\tau}_{xy}}{\partial x} + \frac{\partial \bar{\sigma}_y}{\partial y} + f_y \end{array} \right\} \quad (6)$$

$$\{R_\Gamma(x, y)\} = \{\bar{\tau}\} - \{\hat{n}\} \cdot \{\bar{\sigma}\} = \left\{ \begin{array}{l} \bar{\tau}_x - (\bar{\sigma}_x \hat{n}_x + \bar{\tau}_{xy} \hat{n}_y) \\ \bar{\tau}_y - (\bar{\tau}_{xy} \hat{n}_x + \bar{\sigma}_y \hat{n}_y) \end{array} \right\} \quad (7)$$

In the finite-element method, an approximate solution is sought that forces these residual functions  $\{R_\Omega(x, y)\}$  and  $\{R_\Gamma(x, y)\}$  to be zero in a weighted integral sense:

$$\int_{\Gamma_n} \phi_i \{R_\Gamma\} d\Omega + \int_{\Omega} \phi_i \{R_\Omega\} d\Omega = 0; \quad i = 1, 2, \dots, K \quad (8)$$

where the  $\phi_i$  functions are the weighting functions. The number of weighting functions  $K$  should equal the number of unknown parameters used to construct the approximate solution  $\bar{u}(x, y)$ ,  $\bar{v}(x, y)$ , for then after integration Equation 8 will be simply a set of  $K$  simultaneous algebraic equations that can be solved for the  $K$  unknown parameters.

In the finite-element method, the domain is subdivided into a mesh of subdomains, called finite elements, connected at vertices, called nodes. Within each element, the displacement fields  $\bar{u}(x, y)$  and  $\bar{v}(x, y)$  are interpolated from nodal values of displacements  $u_i$  and  $v_i$  using standard known interpolating polynomial functions called shape functions. Thus, the unknown parameters to be solved for are the displacement components  $u_i$ ,  $v_i$  at each node point  $i$  in the domain. The shape functions associated with each node vary between 0 and 1. Interpolation within an element is achieved by a simple linear combination of the element nodal shape functions multiplied against the element nodal displacements:

$$\bar{u}^e(x, y) = \sum_{i=1}^{M^e} N_i^e(x, y) \mu_i^e \quad (9)$$

$$\tilde{v}^e(x,y) = \sum_{i=1}^{M^e} N_i^e(x,y)v_i^e \quad (10)$$

where  $M^e$  is the number of nodes that define element  $e$  and  $N_i^e(x, y)$  is the shape function associated with node  $i$  of element  $e$ .

Now we return to Equation 8. In the finite-element method, the weighting functions  $\phi_i$  are taken to be the shape functions  $N_i$  used to interpolate the displacement fields  $\tilde{u}(x, y)$  and  $\tilde{v}(x, y)$ . Here,  $N_i$  is the shape function associated with node  $i$  for each displacement component and is the result of a simple piecewise combination of all the element nodal shape functions,  $N_i^e$ , that are connected to node  $i$ . Therefore, for 2D elasticity with two displacement components,  $K = 2N$ , where  $N$  equals the total number of nodes. Further, since the domain is subdivided into finite elements, the boundary and domain integrations shown in Equation 8 can be subdivided into a set of individual element boundary and domain integrations, making the integrations much easier to compute. This also enables each individual finite element to be unique in terms of its material properties and behavior, strain-displacement relationships, body forces, loading conditions, etc. Since finite elements can be as small as necessary to capture the complexity of the problem, the net result is that no matter how complicated the physical domain is in shape, in known material property relationships and behavior, in known loading conditions, and in kinematic constraints, an approximate solution can be obtained via the finite-element method. In general, the limitations that might preclude an acceptably accurate solution from being obtained are lack of knowledge regarding material properties and associated material behavioral laws, uncertainty about kinematic constraints and loading conditions, difficulty in defining necessary geometry, and limitations in computer resources. The method is also based on the concept of continuums and therefore is not applicable at

the atomic level where quantum mechanic effects dominate.

It is important that any approximate solution be capable of converging toward the theoretically exact solution to the governing differential equations and imposed boundary conditions, if such a solution were known. This means that if a sequence of numerical analysis is carried out, with each subsequent analysis having more degrees of freedom (typically realized by refining the mesh with smaller and smaller elements), the method should converge to the theoretically exact solution of the problem being modeled. For properly constructed meshes, this is indeed the case, for Equation 8 forces the residual functions  $\{R_\Omega(x, y)\}$  and  $\{R_\Gamma(x, y)\}$  to be mathematically orthogonal to the weighting functions  $\phi_i$ . With mesh refinement,  $N$ , the number of weighting functions,  $\phi_i$ , increases. Although the weighting functions may be relatively simple polynomials (i.e., linear polynomials if using linear finite elements), as a set they can approximate more complicated functions arbitrarily close. Essentially, this forces the residual functions to be mathematically orthogonal to an increasingly more complicated set of functions. In the limit as  $N \rightarrow \infty$ , the residual functions are forced to be orthogonal to all possible well-behaved functions. This condition only occurs when  $\{R_\Omega(x, y)\} = 0$  and  $\{R_\Gamma(x, y)\} = 0$ . Therefore, an exact solution to the governing problem has been obtained.

Of course, the above discussion addresses only the inherent discretization error in the finite-element method: the representation of the infinite degrees of freedom of the continuum by a finite number of degrees of freedom. Equally and often more important are various modeling errors introduced into the problem. Idealizations of geometry, material property behavior and variability, loading conditions, constraints, etc., all introduce to some extent modeling errors that may or may not significantly affect the analysis result. The analyst must rely on his or her domain expertise and whenever possible employ experimental data to validate finite-element models.